J Mater Sci: Mater Electron (2014) 25:3251–3256
DOI 10.1007/s10854-014-2010-3

Resistive switching in $BiFeO_3$-based heterostructures due to ferroelectric modulation on interface Schottky barriers

Dongxia Chen · Aidong Li · Di Wu

Received: 7 March 2014 / Accepted: 12 May 2014 / Published online: 21 May 2014

Abstract Ferroelectric $BiFeO_3$ (BFO) thin films were deposited on (001) $SrTiO_3$ substrates buffered with $La_{0.7}Sr_{0.3}MnO_3$ (LSMO) electrodes. Bipolar resistive switching in Pt/BFO/LSMO heterostructures were observed with high stability and long retention. However, transport characteristics of Pt/BFO/LSMO is highly asymmetric and pronounced resistive switching can only be observed by applying negative reading pulses on the Pt top electrodes, i.e. when the Pt/BFO Schottky barrier is reverse-biased. This resistive switching is discussed in terms of a modulation on the Pt/BFO interface Schottky barrier by the polarization switching in ferroelectric BFO. Comparative studies on Pt/BFO/$SrRuO_3$ and Pt/BFO/$LaNiO_3$ heterostructures reveal that the work function of the electrode materials and the formation of Schottky barriers are significant to the observed resistive switching behaviors.

1 Introduction

With the continuous miniaturization of electronic devices, traditional semiconductor nonvolatile memories, based on the storage of charges, meet scaling difficulties such as statistical fluctuations and intolerable leakage current [1]. Resistive random access memories, based on the change of resistance under electric pulses, have been proposed as promising candidates for the next generation nonvolatile memories, owing to their high density, high operation speed, low power consumption and simple memory architecture [2, 3].

A variety of materials show resistive switching behaviors obeying different mechanisms [2]. For example, formation and rupture of conductive filaments composed of charged defects have been reported responsible for resistive switching in NiO [4], TiO_2 [5], and $SrZrO_3$ [6]. Mott transition may result in resistive switching in electron-correlated compounds such as VO_2 [7] and $GaTa_4Se_8$ [8]. Electric-driven redistribution of charged defects around the film/electrode interface represents another important resistive switching mechanism because such a redistribution may alter the film/electrode contact. It has been reported that the movement and recombination of oxygen vacancies at the interface dominate the resistive switching in $TiO_{2-\delta}/La_{2/3}Sr_{1/3}MnO_3$ stacks [9].

For the modulation of interface contacts, spontaneous polarization switching in ferroelectric thin films provides an effective and reliable way that does not rely on the movement of charged defects in nanoscale. The ferroelectric bound charges, which can be switched with polarization switching in a nonvolatile manner, can be regarded as additional interfacial charges on the film/electrode interface. The band alignment and contact resistance can then be switched with polarization switching. Jiang et al. [10] and Wang et al. [11, 12] have reported resistive switching due to a switching diode effect in Pt/$BiFeO_3$ (BFO)/$SrRuO_3$ heterostructures. In these heterostructures, the two interface Schottky barriers were modeled as diodes connected back-to-back, in which the ferroelectric polarization drives one forward-biased and the other reverse-biased. The direction of the diodes and the overall resistance can be switched by polarization switching due to the ferroelectric modulation on the carrier

D. Chen · A. Li · D. Wu (✉)
National Laboratory of Solid State Microstructures, Department of Materials Science and Engineering, College of Engineering and Applied Sciences, Nanjing University, Nanjing 210093, China
e-mail: diwu@nju.edu.cn

concentration in the vicinity of the interfaces and barrier height of the Schottky junctions [12].

However, if the mechanism, the ferroelectric modulation on the Schottky barrier, works, one Schottky barrier at the interface is enough to generate a resistive switching. It is not necessary to have two back-to-back Schottky barriers. To confirm this, here we report resistive switching observed in Pt/BFO/$La_{0.7}Sr_{0.3}MnO_3$ (LSMO) heterostructures, in which the BFO/LSMO interface is non-blocking. By comparative studies with $LaNiO_3$ (LNO) and $SrRuO_3$ (SRO) electrodes, we show that the resistive switching can be explained in line with the switching diode scenario [12]. The work function of electrode materials and the formation of interface Schottky barriers are significant to the observed resistive switching.

2 Experimental details

LSMO and BFO films were deposited epitaxially on (001) $SrTiO_3$ (STO) substrates by pulsed laser deposition (AdNaNo Corp.), using a Coherent CompexPro 205F KrF excimer laser with a 248 nm output. The energy density on targets was estimated as $\sim 1.0\,J/cm^2$ and the oxygen pressure was kept around 13 Pa. LSMO electrodes were deposited at 800 °C with 2 Hz laser repetition. BFO films were deposited at 750 °C with 4 Hz repetition. The thickness of BFO is about 50 nm as calibrated by a Zeiss ULTRA 55 field emission scanning electron microscope. Comparative SRO and LNO bottom electrodes were deposited with 5 Pa oxygen pressure at 760 and 650 °C, respectively. The structure was checked by X-ray diffraction (XRD) using a Rigaku ULTIMA-III diffractometer with Cu Kα radiation. Ferroelectric nature of BFO films was characterized by piezoelectric force microscopy (PFM) using an Asylum Research Cypher atomic force microscope. Pt top electrodes, 200 μm in diameter, were sputter-deposited through a shadow mask. Transport measurements were performed using a Keithley 2,400 source-measure unit. The voltage was applied on the Pt top electrodes with the oxide bottom electrodes grounded through a silver paste contact.

3 Results and discussions

Figure 1a shows the XRD pattern of Pt/BFO/LSMO heterostructures deposited on (001) STO substrates. Only (001) peaks from BFO/LSMO/STO stacks can be observed, indicating the epitaxial growth of perovskite LSMO and BFO thin films. Figure 1b shows a cross-section SEM image of a BFO/LSMO/STO sample. Clear BFO/LSMO

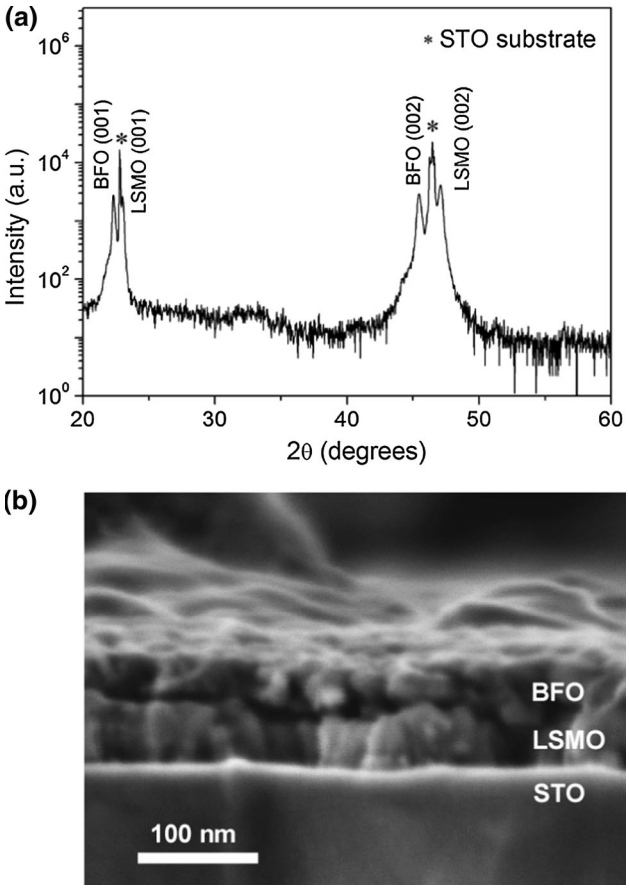

Fig. 1 XRD pattern (**a**) and cross-sectional SEM image (**b**) of BFO/LSMO heterostructures deposited on (001) STO substrates

and LSMO/STO interfaces can be observed. The thickness of BFO is about 51 ± 2 nm averaged from 10 measurements. To study the local ferroelectric properties of BFO thin films by PFM, a triangle wave of 5.0 V in amplitude was applied through a Pt-coated tip (Olympus AC240TM). As shown in Fig. 2a, b, the clear hysteresis in PFM amplitude and phase signals indicates the ferroelectric nature of the BFO thin film. Figure 2c, d show out-of-plane PFM amplitude and phase images of ferroelectric domains written on the BFO surface. Downward domains (with polarization pointing to the bottom electrodes) and upward domains (with polarization pointing to the film surface) were written by scanning the tip biased at 7.0\,V and −8.5\,V, respectively. A checkerboard pattern composed of 4 adjacent 1.5 μm × 1.5 μm upward and downward domains were written. Domain walls of dark contrast can be observed clearly in the amplitude image. It can also be observed that downward domains (purple in the phase image) are preferred in the as-deposited BFO thin films. The images shown were acquired 3 hours after domain patterning. They are essentially the same as those acquired right after domain patterning, indicating good polarization

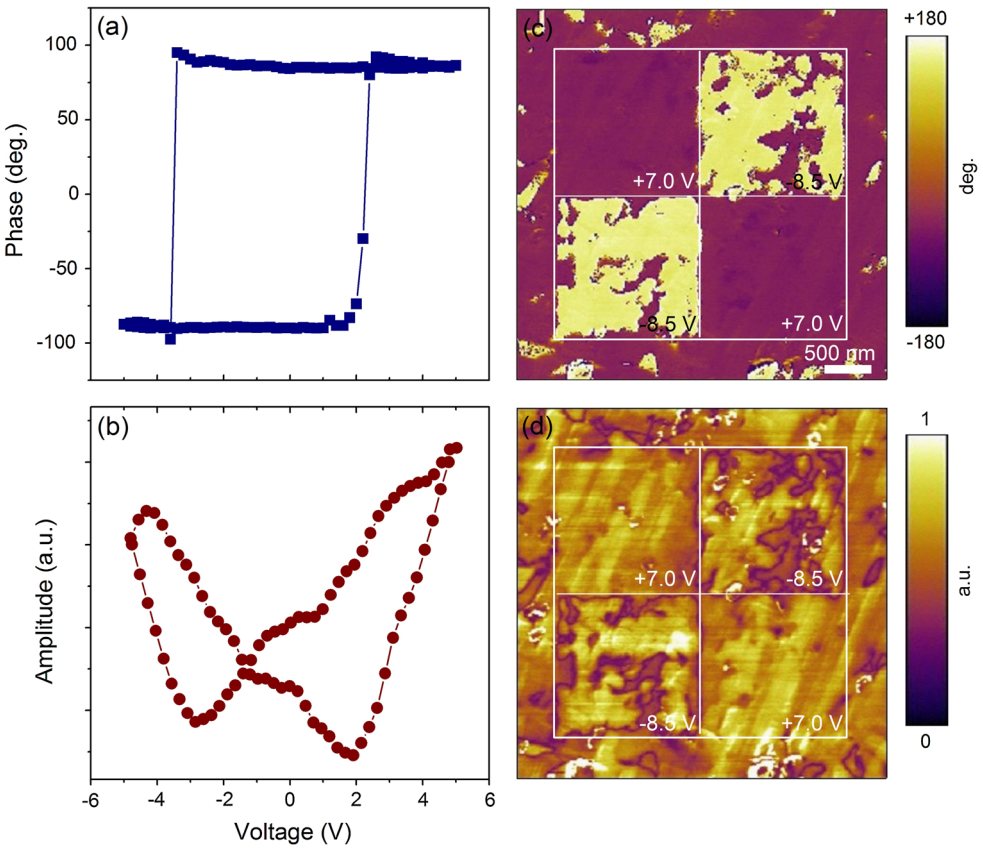

Fig. 2 PFM amplitude (**a**) and phase (**b**) hysteresis loops, amplitude (**c**) and phase (**d**) images of domains written on BFO thin films deposited on LSMO buffered STO substrates. Downward (upward) domains written with a positive (negative) bias are labeled with "+" ("−")

retention. However, there are areas in which polarization can not be switched upward by the applied −8.5 V bias. This may be ascribed to inhomogeneity in the BFO films.

The Pt/BFO/LSMO heterostructures were polarized to downward or upward state. Then current–voltage (I–V) characteristics were measured. Typical I–V curves for upward and downward polarizations are shown in Fig. 3a. The I–V curves are highly asymmetric, especially for the downward polarization state where the heterostructure shows a typical rectifying characteristic. Although the I–V curves in the positive voltage region does not show a clear resistance contrast for the two polarization states, pronounced resistive switching can be observed in the negative voltage region. In Fig. 3b, 20 cycles of I–V curves are displayed in a semi-logarithmic plot. The applied voltage was set to sweep from 0 to 4.0 V, then from 4.0 to −5.0 V and finally from −5.0 back to 0 V, as indicated by arrows in Fig. 3b. A clear hysteresis can be observed in the negative voltage region. The positive voltage drives the polarization in BFO pointing to the bottom electrode and sets the Pt/BFO/LSMO memory cell into the high resistance state, while a negative voltage reset it back to the low resistance state by polarization reversal. The current contrast is about 10, as read at −1.0 V. The identical hysteresis with repetitive cycling, as shown in Fig. 3b, indicates a stable resistive switching. Fig. 3c shows the switching characteristic of Pt/BFO/LSMO heterostructures. Write pulses of 5.0 and −6.0 V in amplitude and 1.0 ms in width were applied alternatively. A read pulse of −1.0 V in amplitude and 100 ms in width was applied after each write pulse. The write-read operation is repeated for more than 1,000 times without failure. Figure 3d shows that data can be retained for more than 10^4 s after the application of a write pulse.

In contrast to the symmetric resistance switching behavior observed in Pt/BFO/SRO heterostructures, pronounced resistive switching can only be sensed by a negative pulse in Pt/BFO/LSMO heterostructures. This can be understood considering that in Pt/BFO/LSMO there is only one Schottky barrier at the Pt/BFO interface. The work function of LSMO is only about 4.8 eV [13, 14], close to that of BFO ($\sim$4.7 eV) [15, 16]. The energy bands at the BFO/LSMO interface is almost flat and the interface is non-blocking [16]. The transport through the heterostructure is mainly controlled by the Pt/BFO interface. The work function of Pt is $\sim$5.3 eV [17], much larger than that of BFO. A Schottky barrier forms at the Pt/BFO interface by electron depletion in n-type BFO [16, 18]. The band diagram in equilibrium, when BFO is not polarized, is shown schematically in Fig. 4a. By solving the Poisson

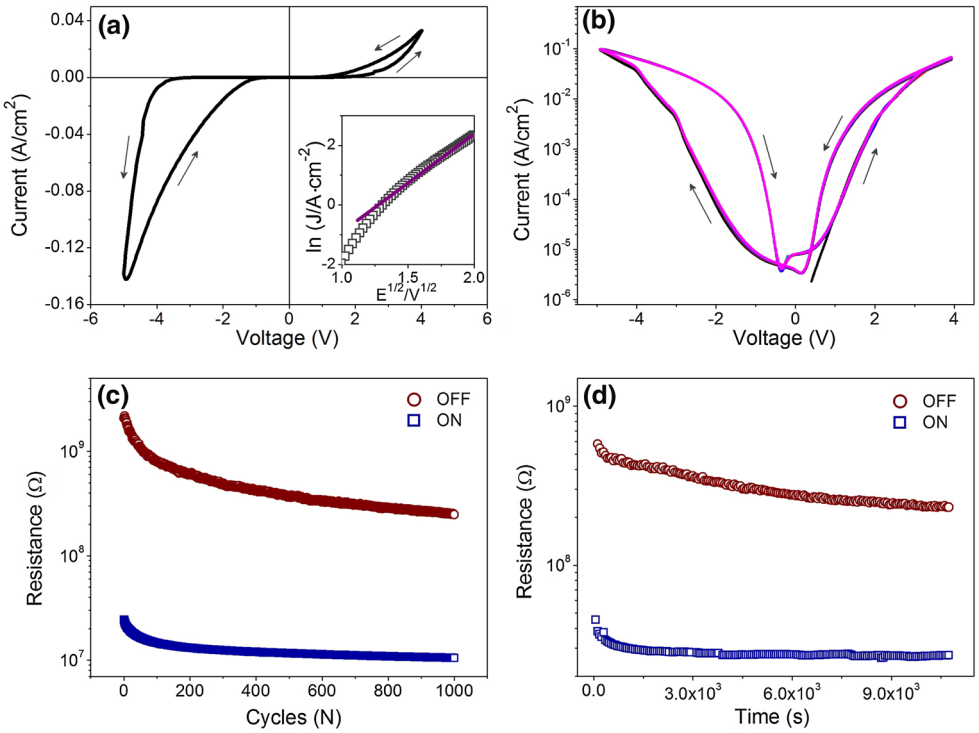

Fig. 3 I–V curves with polarization switched upward and downward (**a**), 20 consecutive I–V cycles (**b**), repetitive resistance switching (**c**), and resistive data retention (**d**) of Pt/BFO/LSMO heterostructures. The *inset* in (**a**) shows that the forward-biased I–V data in high resistance state fitted well to the Schottky emission current. The *arrows* in (**b**) indicate the cycling direction

equation with an abrupt approximation [19], the building potential (ϕ_{bi}) in BFO can be related to the space charge density (Q_{sc}) as,

$$\phi_{bi} = \frac{{Q_{sc}}^2}{2q\epsilon_r N_D}, \tag{1}$$

where q is the electron charge, ϵ_r the dielectric constant and N_D the carrier concentration of BFO. When BFO is polarized, ferroelectric bound charges occur at the interface. These additional charges must be compensated by the space charges in BFO. For downward polarization pointing to LSMO, there are positive bound charges at the Pt/BFO interface. The space charge density with downward polarization is

$$Q_{sc}^{+} = Q_{sc} + P = qN_D w_D + P, \tag{2}$$

where P is the polarization of BFO and w_D is the depletion length in absence of polarization. Following Ge et al. [12], we take $N_D = 4 \times 10^{16}\,\mathrm{cm}^{-3}$ for BFO. Even if the 50 nm thick BFO thin film is fully depleted, $Q_{sc} = qN_D w_D$ is much smaller than the polarization of BFO, which is usually larger than 30 μC/cm^2 [20]. Thus, the building potential with downward polarization becomes,

$$\phi_{bi}^{+} = \frac{P^2}{2q\epsilon_r N_D}, \tag{3}$$

much larger than that without polarization. This is shown schematically in Fig. 4b. Conversely, when the polarization is switched upward pointing to the Pt electrode, the

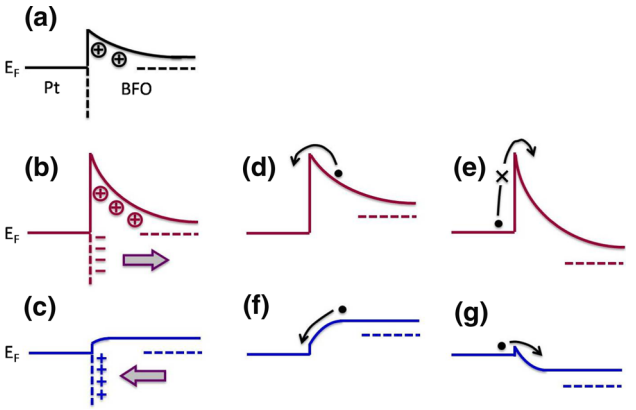

Fig. 4 Schematic band diagrams at the Pt/BFO interface in equilibrium in absence of polarization (**a**), with downward (**b**) and upward (**c**) polarizations. The *circled-plus* symbols represent positive space charges in BFO. *Arrows* in **b**, **c** indicates the direction of ferroelectric polarization. The "+" and "−" symbols represent positive and negative ferroelectric bound charges, respectively, at the interface. **d**, **e** Band diagrams with downward polarization under forward and reverse bias, respectively. **f**, **g** Band diagrams with upward polarization under forward and reverse bias, respectively

strong positive bound charges at the interface drives BFO into electron accumulation, as shown in Fig. 4c. Band diagrams of the Pt/BFO Schottky barrier, with either downward or upward polarization, under forward and reverse bias are also shown in Fig. 4. It is clear that one may have a rectifying characteristic for downward polarization, as observed in Fig. 3a. The I–V curve for

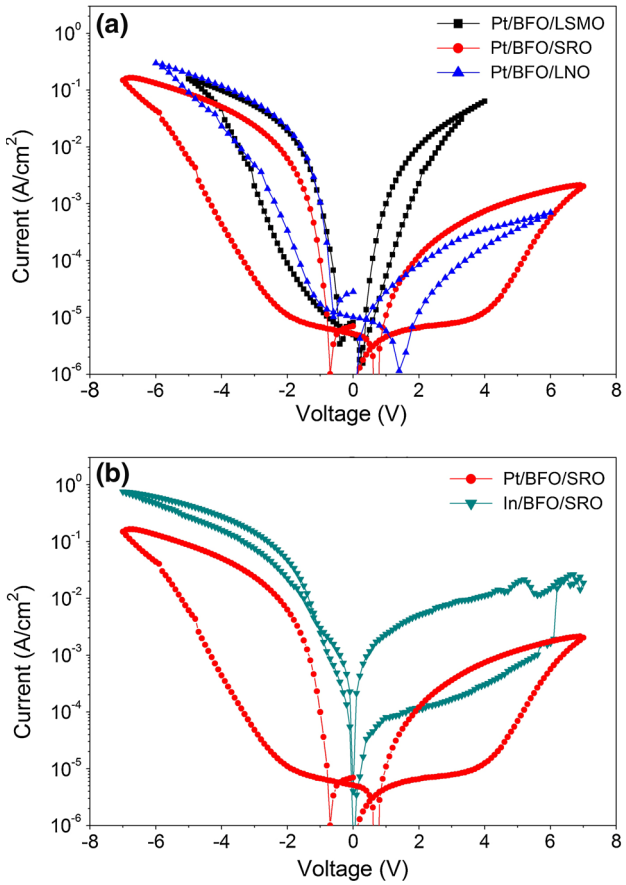

Fig. 5 **a** Comparison among I–V characteristics of Pt/BFO/LSMO, Pt/BFO/LNO, and Pt/BFO/SRO heterostructures; **b** comparison between I–V characteristics of Pt/BFO/SRO and In/BFO/SRO heterostructures

downward polarization under forward bias can be well fitted to the thermal emission current. This is shown in the inset of Fig. 3a. The reverse-biased Pt/BFO Schottky barrier with downward polarization can be used as the high resistance state. However, for upward polarization, current can flow under either bias condition. It can be used as the low resistance state. Pronounced resistance contrast can only be read with a negative pulse, which reverse-biases the Schottky barrier in high resistance state.

To further identify the effect of work function of the bottom electrode, we compare the resistive switching behavior of Pt/BFO/LSMO with those of Pt/BFO/SRO and Pt/BFO/LNO. SRO, with a work function ~ 5.2 eV [17], forms a Schottky barrier at the bottom interface, while LNO, with a work function ~ 4.5 eV [21], forms a Ohmic contact with BFO. Figure 5a shows I–V hysteresis of the three heterostructures. The heterostructure with SRO bottom electrode shows pronounced I–V hysteresis in both positive and negative voltage sides. This is because the Schottky barrier at BFO/SRO interface is also modulated by the ferroelectric polarization. However, I–V characteristics of the heterostructure with LNO bottom electrode are similar to that with LSMO bottom electrode. Since the non-blocking bottom interface is not sensitive to ferroelectric polarization reversal, pronounced I–V hysteresis appears only in the negative voltage side when the Pt/BFO Schottky barrier is reverse-biased. Interestingly, as the high work function top electrode in Pt/BFO/SRO is replaced by low work function Indium, the I–V hysteresis in negative voltage disappears in In/BFO/SRO, as shown in Fig. 5b.

4 Summary

We have shown ferroelectric resistive switching behaviors in BFO-based heterostructures with Pt top electrodes and LSMO, SRO and LNO bottom electrodes. Long data retention and stable resistive switching have been demonstrated in Pt/BFO/LSMO. The resistive switching can be explained in terms of ferroelectric modulation on the interface Schottky barriers, i.e. the switching diode scenario proposed previously [10–12]. The work function of the electrode materials and the formation of Schottky barrier at the interface are found significant to achieve pronounced resistive switching. BFO interfaces with low work function LSMO, LNO and In contribute little to the resistive switching, while BFO interfaces with high work function Pt and SRO show pronounced resistive switching.

Acknowledgments This work was jointly sponsored by the Natural Science Foundation of China (51222206 and 11374139), the Natural Science Foundation of Jiangsu Province (BK2012016) and the Doctoral Foundation of Ministry of Education of China (20110091110013).

References

1. R. Waser, R. Dittmann, G. Staikov, K. Szot, Adv. Mater. **21**, 2632 (2009)
2. J.J. Yang, I.H. Inoue, T. Mikolajick, C.S. Hwang, MRS Bull. **37**, 131 (2012)
3. R. Waser, M. Aono, Nat. Mater. **6**, 833 (2007)
4. L. Goux, R. Degraeve, J. Meersschaut, B. Govreanu, D.J. Wouters, S. Kubicek, M. Jurczak, J. Appl. Phys. **113**, 054505 (2013)
5. D.H. Kwon, K.M. Kim, J.H. Jang, J.M. Jeon, M.H. Lee, G.H. Kim, X.S. Li, G.S. Park, B. Lee, S.W. Han, M. Kim, C.S. Hwang, Nat. Nanotechnol. **5**, 148 (2010)
6. M.H. Lin, M.C. Wu, C.H. Lin, T.Y. Tseng, J. Appl. Phys. **107**, 124117 (2010)
7. J. Kim, C. Ko, A. Frenzel, S. Ramanathan, J.E. Hoffman, Appl. Phys. Lett. **96**, 213106 (2010)
8. V. Dubost, T. Cren, C. Vaju, L. Cario, B. Corraze, E. Janod, F. Debontridder, D. Roditchev, Nano Lett. **13**, 3648 (2013)
9. Y.S. Chen, B. Chen, B. Gao, L.P. Chen, G.J. Lian, L.F. Liu, Y. Wang, X.Y. Liu, J.F. Kang, Appl. Phys. Lett. **99**, 072113 (2011)
10. A.Q. Jiang, C. Wang, K.J. Jin, X.B. Liu, J.F. Scott, C.S. Hwang, T.A. Tang, H.B. Lu, G.Z. Yang, Adv. Mater. **23**, 1277 (2011)
11. C. Wang, K.J. Jin, Z.T. Xu, L. Wang, C. Ge, H.B. Lu, H.Z. Guo, M. He, G.Z. Yang, Appl. Phys. Lett. **98**, 192901 (2011)

12. C. Ge, K.J. Jin, C. Wang, H.B. Lu, C. Wang, G.Z. Yang, Appl. Phys. Lett. **99**, 063509 (2011)
13. M. Minohara, I. Ohkuho, H. Kumigashira, M. Oshima, Appl. Phys. Lett. **90**, 132123 (2007)
14. W. Reagor, S.Y. Lee, Y. Li, Q.X. Jia, J. Appl. Phys. **95**, 7971 (2004)
15. H. Yang, H.M. Luo, H. Wang, I.O. Usov, N.A. Suvorova, M. Jain, D.M. Feldmann, P.C. Dowden, R.F. DePaula, Q.X. Jia, Appl. Phys. Lett. **92**, 102113 (2008)
16. Y. Zhou, X. Zou, L. You, R. Guo, Z.S. Lim, L. Chen, G.L. Yuan, J.L. Wang, Appl. Phys. Lett. **104**, 012903 (2014)
17. R. Plonka, R. Dittmann, N.A. Pertsev, E. Vasco, R. Waser, Appl. Phys. Lett. **86**, 202908 (2005)
18. S.J. Clark, J. Robertson, Appl. Phys. Lett. **90**, 132903 (2007)
19. S.M. Sze, K.K. Ng, *Physics of Semiconductor Devices*, 3rd edn. (Wiley, New York, 2007), p. 137
20. J. Wang, J.B. Neaton, H. Zheng, V. Nagarajan, S.B. Ogale, B. Liu, D. Viehland, V. Vaithyanathan, D.G. Schlom, U.V. Waghmare, N.A. Spaldin, K.M. Rabe, M. Wuttig, R. Ramesh, Science **299**, 1719 (2003)
21. T.-H. Yang, Y.-W. Harn, K.-C. Chiu, C.-L. Fana, J.-M. Wu, J. Mater. Chem. **22**, 17071 (2012)